

Cross-Species Data Integration for Enhanced Layer Segmentation in Kidney Pathology

Junchao Zhu^a, Mengmeng Yin^b, Ruining Deng^a, Yitian Long^d, Yu Wang^b, Yaohong Wang^c, Shilin Zhao^c, Haichun Yang^b, and Yuankai Huo^{*a,b,d}

^aDepartment of Computer Science, Vanderbilt University, Nashville, TN, USA

^bDepartment of Pathology, Microbiology and Immunology, Vanderbilt University Medical Center, Nashville, TN, USA

^cDepartment of Biostatistics, Vanderbilt University Medical Center, Nashville, TN, USA

^dData Science Institute, Vanderbilt University, Nashville, TN, USA

ABSTRACT

Accurate delineation of the boundaries between the renal cortex and medulla is crucial for subsequent functional structural analysis and disease diagnosis. Training high-quality deep-learning models for layer segmentation relies on the availability of large amounts of annotated data. However, due to the patient's privacy of medical data and scarce clinical cases, constructing pathological datasets from clinical sources is relatively difficult and expensive. Moreover, using external natural image datasets introduces noise during the domain generalization process. Cross-species homologous data, such as mouse kidney data, which exhibits high structural and feature similarity to human kidneys, has the potential to enhance model performance on human datasets. In this study, we incorporated the collected private Periodic Acid-Schiff (PAS) stained mouse kidney dataset into the human kidney dataset for joint training. The results showed that after introducing cross-species homologous data, the semantic segmentation models based on CNN and Transformer architectures achieved an average increase of 1.77% and 1.24% in mIoU, and 1.76% and 0.89% in Dice score for the human renal cortex and medulla datasets, respectively. This approach is also capable of enhancing the model's generalization ability. This indicates that cross-species homologous data, as a low-noise trainable data source, can help improve model performance under conditions of limited clinical samples. Code is available at https://github.com/hrlblab/layer_segmentation.

Keywords: Layer Segmentation, Kidney, Pathology Image, Cross-Species Data

1. INTRODUCTION

A kidney biopsy can provide important information about a patient's kidney function and is a crucial standard for diagnosing kidney-related diseases.¹ During histopathological analysis of kidney biopsy tissues, precise localization of the boundary between the cortex and medulla layers is essential for subsequent functional structural analysis (such as the glomerulus).^{2,3} Moreover, the renal cortex and medulla play distinct roles in maintaining bodily homeostasis.⁴ Changes in the boundaries and proportions of the renal cortex and medulla are associated with the occurrence and progression of diseases such as chronic kidney disease and renal tumors.^{5,6} In clinical practice, this process is typically performed by experienced doctors through visual inspection under a microscope. However, due to the large size of histopathological images, manually observing and localizing the layers of kidney tissue under a microscope is time-consuming and labor-intensive, which motivates people to develop efficient automated tools.

In recent years, data-driven deep-learning methods⁷⁻⁹ have introduced new tools for clinical computer-aided diagnosis, significantly improving diagnostic efficiency and accuracy. The popularity of convolutional neural networks (CNNs) and Transformer architectures has contributed to a variety of clinical practices,^{10,11} including the segmentation of retinal fundus images¹² and the diagnosis of breast cancer.¹³ In the field of kidney diseases, deep-learning models have been employed to identify and segment glomerular structures in human kidney biopsies. However, training high-quality neural network models demands a substantial amount of high-quality

Corresponding author: Yuankai Huo: E-mail: yuankai.huo@vanderbilt.edu

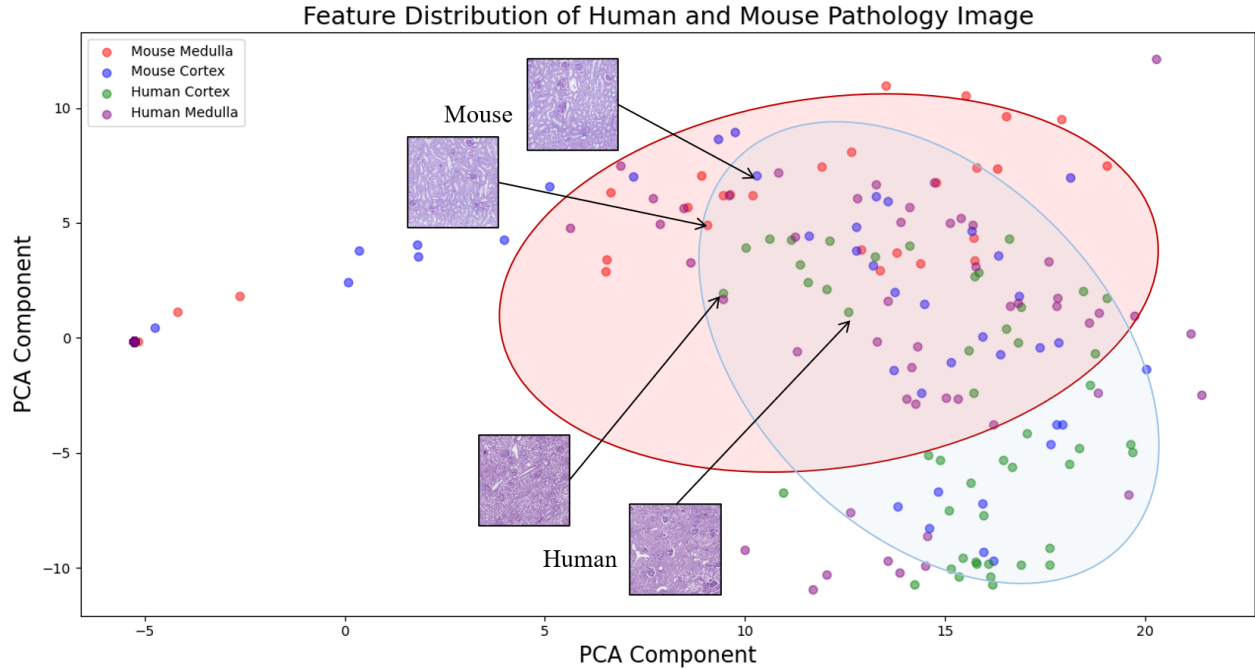


Figure 1: The feature distribution of the cortex and medulla in human and mouse kidney images at the patch level. Human and mouse data points have a high overlap in the PCA space, indicating a high degree of cross-species similarity in the homologous tissue structure.

annotated data. In the medical field, data collection from humans is particularly challenging due to medical ethics reviews and patient privacy concerns.

To address this issue, seeking relevant external data has become a potential approach. Some studies have improved the performance of medical image classification by using transfer learning with models pre-trained on natural images (e.g., ImageNet).¹⁴ However, due to the unique staining styles and tissue structures of histopathology images, noise may be introduced during domain generalization. In contrast, homologous organs across species have functional and structural similarities. Some studies have shown a high degree of similarity between human and mouse kidney tissues,¹⁵ with common features such as localized lesions and inflammatory tissues found in pathological conditions like kidney tumors and diabetic nephropathy in both species.^{16,17}

The feature distribution of the cortex and medulla in human and mouse kidney images at the patch level is shown in Figure 1. We extracted features from 50 histopathological images of human and mouse kidneys by ResNet50 and then reduced the dimension of features by performing the principal component analysis (PCA). The figure shows a high degree of overlap between the data points of humans and mice in the PCA space, indicating a high cross-species similarity in these two image regions. Therefore, data from homologous organs across species may improve model performance and generalization ability on human datasets.

In this study, we demonstrated that incorporating cross-species homologous data for collaborative training can enhance the performance of models in segmenting the cortex and medulla in human kidney histopathology images. We combined a private mouse kidney dataset stained with Periodic Acid-Schiff (PAS) with human kidney datasets for joint training. Compared with training on each dataset separately, the cross-species mixed data training achieved performance improvements across all targets in mainstream CNN and Transformer-based segmentation networks. This approach allows the model to leverage knowledge from the mouse dataset and adapt it to the human dataset, thereby improving segmentation performance and generalization capabilities

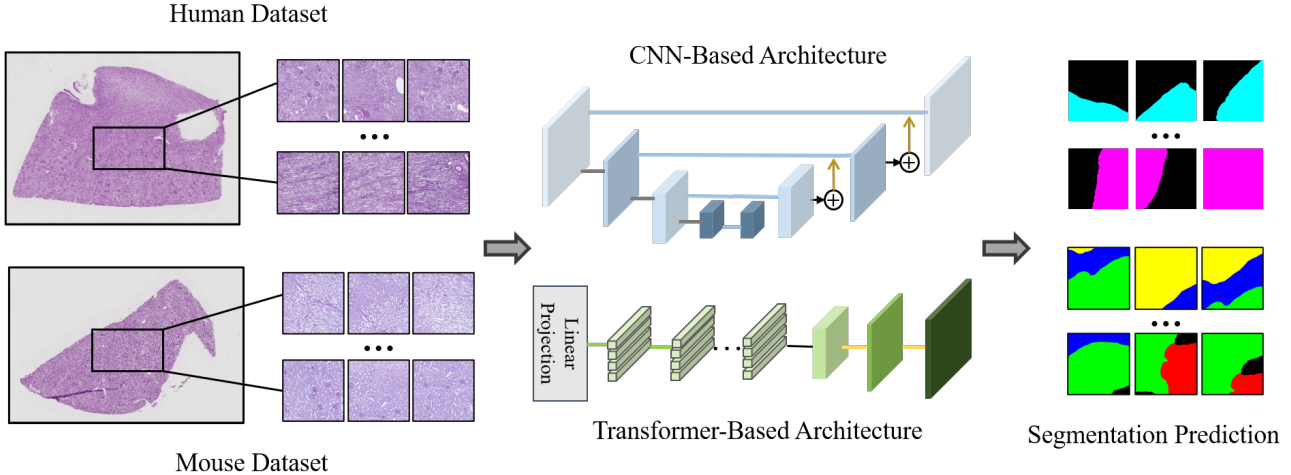


Figure 2: Framework of the Cross-Species Training Process: Patches are first extracted from WSIs and then are utilized to train and test across several baseline models, which includes individual treatments for each species' data as well as combined data processing.

2. METHOD

2.1 Cross-species Training Framework

Before training the model, we first annotated the boundaries between the cortex and medulla at the whole slide image (WSI) level in the human and mouse datasets, completing the annotations for semantic segmentation. Subsequently, we cropped the WSIs into 1024×1024 pixel patches. These patches are then used to train and test several baseline models, including separate treatments for each species' data as well as combined training processing.

The training process is split into two distinct parts when training independently, including a four-class segmentation task for the mouse kidney dataset and single-category segmentation tasks for two categories within the human kidney dataset. To handle this diversity, we employ a hybrid loss function that combines Cross Entropy Loss (CE) and Dice Loss. Cross Entropy Loss evaluates the classification accuracy of each pixel in multi-class segmentation tasks, while Dice Loss quantifies the overall similarity between the predictions y' and the ground truth y . Thus, the hybrid loss function L_s in independent training can be stated as:

$$L_s = \lambda_1 * CE(y, y') + \lambda_2 * Dice(y, y') \quad (1)$$

where λ_1 and λ_2 are hyperparameters used to balance the two losses.

While training with cross-species data, the model's training process equates to handling a segmentation task with seven categories. Notably, the medulla category in the human dataset has significantly fewer images compared with other categories. To address this class imbalance, we have replaced traditional Cross Entropy Loss with Focal Loss (FL) during the mixed training process. Additionally, we have implemented a specific weight w_i for each category i within the Focal Loss framework, thereby boosting the model's ability to effectively handle imbalanced data by focusing more on the rare categories. Consequently, the overall loss function L_t with hyperparameters λ_3 and λ_4 during joint training can be described as:

$$L_t = \lambda_3 * w_i * FL(y, y') + \lambda_4 * Dice(y, y') \quad (2)$$

2.2 Baseline

2.2.1 CNN-based Method

To evaluate the effectiveness of cross-species homologous data on human kidney layer segmentation, we selected three CNN-based baseline models: U-Net,⁸ tailored for medical image segmentation, alongside DeepLabv3+¹⁸

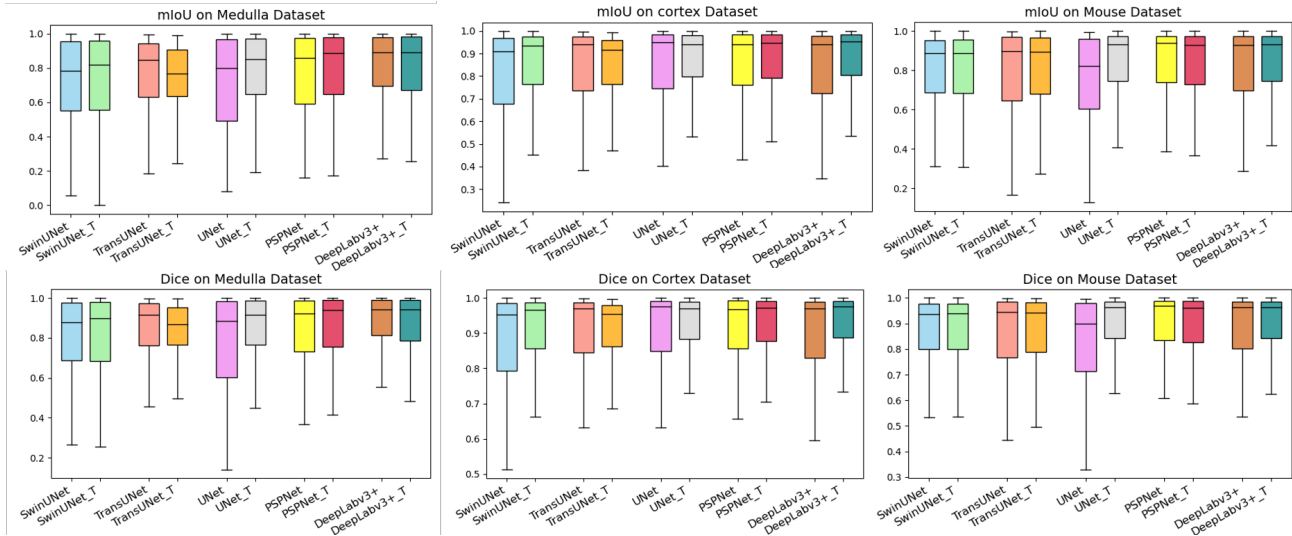


Figure 3: The distribution of mIoU and Dice score across test datasets by different training manner. The collaborative training approach led to a more concentrated distribution of these metrics.

and Pyramid Scene Parsing Net (PSPNet),¹⁹ both utilized for general image segmentation. We employed ResNet50⁷ as the backbone for both U-Net and PSPNet to enhance feature extraction, while opting for MobileNetV2²⁰ as the backbone for DeepLabv3+.

2.2.2 Transformer-based Method

Transformer-based architectures have emerged as a prominent choice in the field since the appearance of the Vision Transformer (ViT).²¹ To assess the feasibility of our method across diverse network architectures, we selected two transformer-based models for evaluation: TransUNet²² and SwinUNet.²³ Specifically, we utilized ViT as the backbone for TransUNet, and Swin Transformer Tiny²⁴ for SwinUNet. Therefore, we can explore how cross-species homologous data performs on Transformer networks of varying parameter scales.

3. EXPERIMENTS

3.1 Data

We collected a private PAS-stained pathology dataset comprising human and mouse kidney tissues sourced from both clinical and laboratory. For the human part, we obtained 27 WSIs from non-cancerous regions of nephrectomy samples. These images were scanned at 20X magnification and annotated by three professional clinicians using QuPath,²⁵ mapping out the contours of the medulla and cortex. Specific binary masks for both the cortex and medulla were derived from these contours.

In the case of the mouse dataset, we acquired 30 renal pathology slides from male mice, including the wild-type mice, mice on the BKS background, and mice treated with an angiotensin receptor blocker. These images were scanned at 40X magnification and detailed annotated by clinicians in QuPath, marking the part of the inner medulla, inner stripe, outer stripe, and cortex.

Both datasets were initially divided into training and testing sets with a 7:3 ratio at the WSI level. Then, labels and whole slide images were segmented into 1024×1024 pixel patches. For the human dataset, this included 1,447 patches from the medulla and 2,714 from the cortex; the mouse dataset comprised 5,012 patches in total.

Table 1: The quantitative performance of models on various datasets with different training methods. Compared with training independently, there is an average improvement of 1.77% and 1.24% in mIoU, along with 1.76% and 0.89% in Dice score on the human cortex and medulla datasets respectively.

Model	Dataset	Separate	Together	mIoU	Dsc	std IoU	std Dsc
UNet ⁸	mouse	✓		0.7644	0.8282	0.0438	0.0322
			✓	0.8594	0.8927	0.0316	0.0187
		✓		0.7163	0.7874	0.0704	0.0495
	medulla		✓	0.7860	0.8477	0.0452	0.0310
		✓		0.8405	0.8851	0.0461	0.0314
			✓	0.8458	0.9034	0.0279	0.0212
PSPNet ¹⁹	mouse	✓		0.8495	0.8958	0.0290	0.0186
			✓	0.8412	0.8891	0.0296	0.0196
		✓		0.7767	0.8375	0.0503	0.0353
	medulla		✓	0.7972	0.8505	0.0457	0.0328
		✓		0.8406	0.8853	0.0433	0.0303
			✓	0.8551	0.8962	0.0361	0.0255
DeepLabv3+ ¹⁸	mouse	✓		0.8308	0.8810	0.0336	0.0217
			✓	0.8509	0.8973	0.0255	0.0165
		✓		0.8130	0.8701	0.0391	0.0255
	medulla		✓	0.8042	0.8580	0.0458	0.0323
		✓		0.8325	0.8780	0.0436	0.0314
			✓	0.8667	0.9062	0.0331	0.0226
TransUNet ²²	mouse	✓		0.8022	0.8566	0.0405	0.0288
			✓	0.8099	0.8629	0.0319	0.0256
		✓		0.7785	0.8503	0.0361	0.0231
	medulla		✓	0.7454	0.8259	0.0359	0.0256
		✓		0.8349	0.8825	0.0382	0.0268
			✓	0.8330	0.8845	0.0351	0.0237
SwinUNet ²³	mouse	✓		0.8105	0.8701	0.0306	0.0199
			✓	0.8124	0.8707	0.0304	0.02
		✓		0.7273	0.7998	0.0611	0.0443
	medulla		✓	0.7410	0.8076	0.0614	0.0470
		✓		0.8016	0.8563	0.0527	0.0383
			✓	0.8379	0.8849	0.0419	0.0291

3.2 Implementation

The experiments were conducted on 4 NVIDIA Tesla V100 GPU cards. We employed an SGD optimizer to configure with a momentum of 0.9 and a weight decay parameter set at 10^{-4} . The initial learning rate, denoted as lr_0 , was established at 1×10^{-3} . A cosine decay strategy is applied to reduce the learning rate to 0.01 of the initial rate during the training process. We have fine-tuned the hyperparameters λ_1 , λ_2 , λ_3 , and λ_4 in our hybrid loss function to values of 0.5, 0.75, 0.75, and 1.0, respectively. Additionally, within the Focal loss component, we adjusted the weights for the human cortex and medulla to 1.25 and 2.0, respectively, while setting the weights for other categories to 1.

4. RESULTS

The evaluation metrics used were Mean Intersection over Union (mIoU) and Dice score, with higher values indicating better semantic segmentation performance. The quantitative performance of models is presented in Table. 1. By integrating homologous mouse kidney data with human datasets for combined training, all models demonstrated an average improvement of 1.77% and 1.24% in mIoU, along with 1.76% and 0.89% in Dice

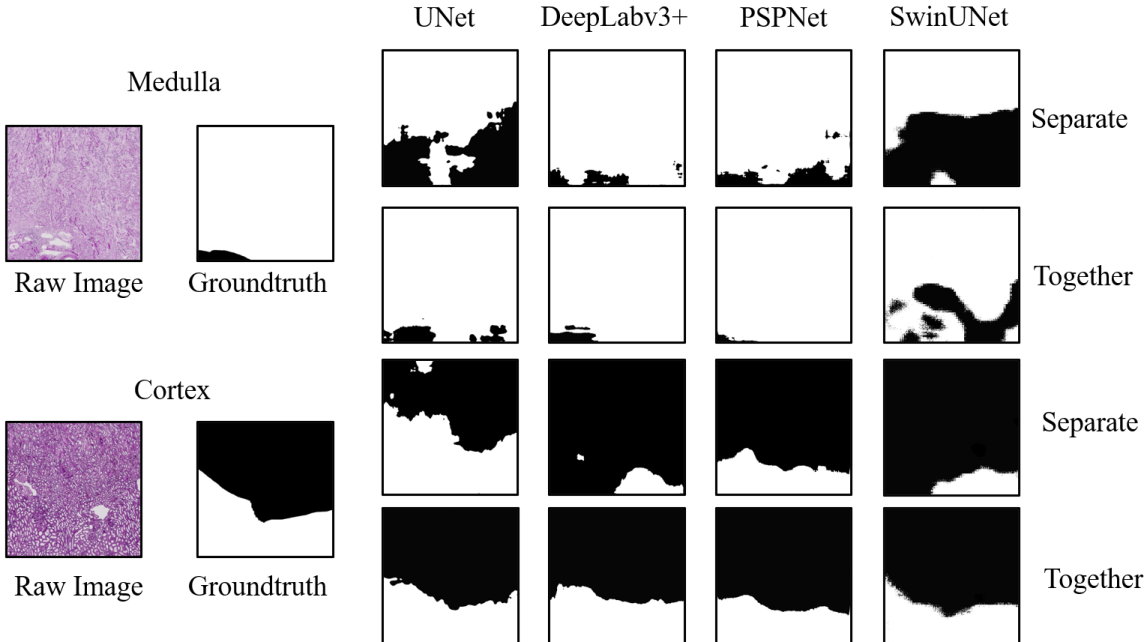


Figure 4: The qualitative outcomes of models on various datasets. By utilizing external homologous data, the models have become better at perceiving edge textures, thus performing better in more precise localization and identification of kidney layer boundaries.

score on the human cortex and human medulla datasets respectively. The distribution of mIoU and Dice score across testsets before and after joint training is depicted in the boxplot in Figure. 3. The collaborative training approach led to a more concentrated distribution of these metrics. Further, observing changes in the standard deviations of mIoU and Dice score in Table. 1, the incorporation of cross-species homologous data markedly enhanced the segmentation performance of both CNN-based and Transformer-based models in human kidney layer segmentation, and also significantly boosted the generalization capabilities of models.

Figure. 4 displays the qualitative outcomes of models on various datasets. Incorporating external homologous data has improved the models' capacity for edge texture perception, which has led to more accurate localization and identification of kidney layer boundaries, thereby enhancing overall model performance.

5. CONCLUSION

In this study, we demonstrated that cross-species homologous data can enhance layer segmentation in the human kidney. Mouse kidney data, with its high structural and staining similarity, significantly improved the semantic segmentation performance of both CNN and Transformer-based models on the human medulla and cortex layers and also boosted the models' generalization abilities. This finding opens up new avenues for medical image analysis by providing an alternative source of data. Integrating homologous data from different species into studies that focus on a single species can extend the pool of low-noise, trainable data. This reduces the limitations imposed by privacy concerns in medical data on human disease research and allows for a better understanding and simulation of complex biological processes when clinical samples are limited.

ACKNOWLEDGMENTS

This research was supported by NIH R01DK135597(Huo), DoD HT9425-23-1-0003(HCY), NIH NIDDK DK56942 (ABF). This work was also supported by Vanderbilt Seed Success Grant, Vanderbilt Discovery Grant, and VISE Seed Grant. This project was supported by The Leona M. and Harry B. Helmsley Charitable Trust grant G-1903-03793 and G-2103-05128. This research was also supported by NIH grants R01EB033385, R01DK132338,

REB017230, R01MH125931, and NSF 2040462. We extend gratitude to NVIDIA for their support by means of the NVIDIA hardware grant.

REFERENCES

- [1] Hogan, J. J., Mocanu, M., and Berns, J. S., “The native kidney biopsy: update and evidence for best practice,” *Clinical Journal of the American Society of Nephrology* **11**(2), 354–362 (2016).
- [2] Stevens, L. A., Coresh, J., Greene, T., and Levey, A. S., “Assessing kidney function—measured and estimated glomerular filtration rate,” *New England Journal of Medicine* **354**(23), 2473–2483 (2006).
- [3] Rosenberg, A. Z. and Kopp, J. B., “Focal segmental glomerulosclerosis,” *Clinical Journal of the American Society of Nephrology* **12**(3), 502–517 (2017).
- [4] Dumas, S. J., Meta, E., Borri, M., Luo, Y., Li, X., Rabelink, T. J., and Carmeliet, P., “Phenotypic diversity and metabolic specialization of renal endothelial cells,” *Nature Reviews Nephrology* **17**(7), 441–464 (2021).
- [5] Windpessl, M., Kostopoulou, M., Conway, R., Berke, I., Bruchfeld, A., Soler, M. J., Sester, M., and Kronbichler, A., “Preventing infections in immunocompromised patients with kidney diseases: vaccines and antimicrobial prophylaxis,” *Nephrology Dialysis Transplantation* **38**(Supplement_2), ii40–ii49 (2023).
- [6] Wolf, M., de Boer, A., Sharma, K., Boor, P., Leiner, T., Sunder-Plassmann, G., Moser, E., Caroli, A., and Jerome, N. P., “Magnetic resonance imaging t1-and t2-mapping to assess renal structure and function: a systematic review and statement paper,” *Nephrology Dialysis Transplantation* **33**(suppl_2), ii41–ii50 (2018).
- [7] He, K., Zhang, X., Ren, S., and Sun, J., “Deep residual learning for image recognition,” in [*Proceedings of the IEEE conference on computer vision and pattern recognition*], 770–778 (2016).
- [8] Ronneberger, O., Fischer, P., and Brox, T., “U-net: Convolutional networks for biomedical image segmentation,” in [*Medical image computing and computer-assisted intervention—MICCAI 2015: 18th international conference, Munich, Germany, October 5–9, 2015, proceedings, part III 18*], 234–241, Springer (2015).
- [9] Ke, J., Lu, Y., Shen, Y., Zhu, J., Zhou, Y., Huang, J., Yao, J., Liang, X., Guo, Y., Wei, Z., et al., “Clusterseg: A crowd cluster pinpointed nucleus segmentation framework with cross-modality datasets,” *Medical Image Analysis* **85**, 102758 (2023).
- [10] Zhu, J., Shen, Y., Zhang, H., and Ke, J., “An anti-biased tbsrtc-category aware nuclei segmentation framework with a multi-label thyroid cytology benchmark,” in [*International Conference on Medical Image Computing and Computer-Assisted Intervention*], 580–590, Springer (2023).
- [11] Ke, J., Zhu, J., Yang, X., Zhang, H., Sun, Y., Wang, J., Lu, Y., Shen, Y., Liu, S., Jiang, F., et al., “Tshfna-examiner: A nuclei segmentation and cancer assessment framework for thyroid cytology image,” *Journal of Shanghai Jiaotong University (Science)* **29**(6), 945–957 (2024).
- [12] Ting, D. S. W., Cheung, C. Y.-L., Lim, G., Tan, G. S. W., Quang, N. D., Gan, A., Hamzah, H., Garcia-Franco, R., San Yeo, I. Y., Lee, S. Y., et al., “Development and validation of a deep learning system for diabetic retinopathy and related eye diseases using retinal images from multiethnic populations with diabetes,” *Jama* **318**(22), 2211–2223 (2017).
- [13] Adam, R., Dell’Aquila, K., Hodges, L., Maldjian, T., and Duong, T. Q., “Deep learning applications to breast cancer detection by magnetic resonance imaging: a literature review,” *Breast Cancer Research* **25**(1), 87 (2023).
- [14] Kim, H. E., Cosa-Linan, A., Santhanam, N., Jannesari, M., Maros, M. E., and Ganslandt, T., “Transfer learning for medical image classification: a literature review,” *BMC medical imaging* **22**(1), 69 (2022).
- [15] Lindström, N. O., McMahon, J. A., Guo, J., Tran, T., Guo, Q., Rutledge, E., Parvez, R. K., Saribekyan, G., Schuler, R. E., Liao, C., et al., “Conserved and divergent features of human and mouse kidney organogenesis,” *Journal of the American Society of Nephrology* **29**(3), 785–805 (2018).
- [16] Burhans, M. S., Hagman, D. K., Kuzma, J. N., Schmidt, K. A., and Kratz, M., “Contribution of adipose tissue inflammation to the development of type 2 diabetes mellitus,” *Comprehensive Physiology* **9**(1), 1 (2018).
- [17] Sato, Y., Boor, P., Fukuma, S., Klinkhammer, B. M., Haga, H., Ogawa, O., Floege, J., and Yanagita, M., “Developmental stages of tertiary lymphoid tissue reflect local injury and inflammation in mouse and human kidneys,” *Kidney International* **98**(2), 448–463 (2020).

- [18] Chen, L.-C., Papandreou, G., Schroff, F., and Adam, H., “Rethinking atrous convolution for semantic image segmentation,” *arXiv preprint arXiv:1706.05587* (2017).
- [19] Zhao, H., Shi, J., Qi, X., Wang, X., and Jia, J., “Pyramid scene parsing network,” in [*Proceedings of the IEEE conference on computer vision and pattern recognition*], 2881–2890 (2017).
- [20] Sandler, M., Howard, A., Zhu, M., Zhmoginov, A., and Chen, L.-C., “Mobilenetv2: Inverted residuals and linear bottlenecks,” in [*Proceedings of the IEEE conference on computer vision and pattern recognition*], 4510–4520 (2018).
- [21] Dosovitskiy, A., Beyer, L., Kolesnikov, A., Weissenborn, D., Zhai, X., Unterthiner, T., Dehghani, M., Minderer, M., Heigold, G., Gelly, S., et al., “An image is worth 16x16 words: Transformers for image recognition at scale,” *arXiv preprint arXiv:2010.11929* (2020).
- [22] Chen, J., Lu, Y., Yu, Q., Luo, X., Adeli, E., Wang, Y., Lu, L., Yuille, A. L., and Zhou, Y., “Transunet: Transformers make strong encoders for medical image segmentation,” *arXiv preprint arXiv:2102.04306* (2021).
- [23] Cao, H., Wang, Y., Chen, J., Jiang, D., Zhang, X., Tian, Q., and Wang, M., “Swin-unet: Unet-like pure transformer for medical image segmentation,” in [*European conference on computer vision*], 205–218, Springer (2022).
- [24] Liu, Z., Lin, Y., Cao, Y., Hu, H., Wei, Y., Zhang, Z., Lin, S., and Guo, B., “Swin transformer: Hierarchical vision transformer using shifted windows,” in [*Proceedings of the IEEE/CVF international conference on computer vision*], 10012–10022 (2021).
- [25] Humphries, M., Maxwell, P., and Salto-Tellez, M., “Qupath: The global impact of an open source digital pathology system,” *Computational and Structural Biotechnology Journal* **19**, 852–859 (2021).